Controlled Grafting of Tetrathiafulvalene (TTF) Containing Diacetylenic Units on Hydrogen-Terminated Silicon Surfaces: From Redox-Active TTF Monolayer to Polymer Films

ARTICLE *in* THE JOURNAL OF PHYSICAL CHEMISTRY C · JUNE 2012

Impact Factor: 4.77 · DOI: 10.1021/jp302041z

5 AUTHORS, INCLUDING:

Bruno Fabre
Université de Rennes 1
127 PUBLICATIONS **1,742** CITATIONS
SEE PROFILE

Dominique Lorcy
Université de Rennes 1
124 PUBLICATIONS **1,638** CITATIONS
SEE PROFILE

THE JOURNAL OF PHYSICAL CHEMISTRY C

Article

pubs.acs.org/JPCC

Controlled Grafting of Tetrathiafulvalene (TTF) Containing Diacetylenic Units on Hydrogen-Terminated Silicon Surfaces: From Redox-Active TTF Monolayer to Polymer Films

Gilles Yzambart, Bruno Fabre,* Franck Camerel, Thierry Roisnel, and Dominique Lorcy*

Sciences Chimiques de Rennes, UMR 6226 CNRS-Université de Rennes 1, MaCSE, Campus de Beaulieu, 35042 Rennes Cedex, France

Supporting Information

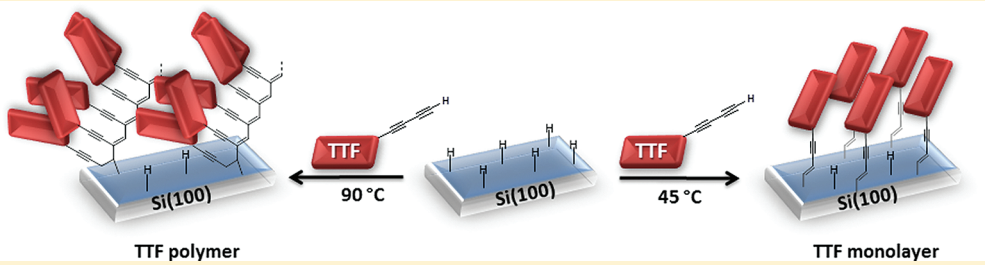

ABSTRACT: A tetrathiafulvalene (TTF)-terminated butadiyne derivative was synthesized and used for the preparation of redox-active TTF-modified hydrogen-terminated oxide-free silicon (Si−H) surfaces. TTF monolayer-modified silicon surfaces were produced when low grafting temperatures were used (typically 45 °C), whereas higher temperatures (90 °C) led to TTF polymer-modified surfaces. IR spectroscopy characterization provided evidence that TTF units bound to the surface through the formation of enyne linkers via hydrosilylation of the terminal alkyne bond. The TTF monolayers prepared at 45 °C were densely packed with a surface coverage of ca. 5.4×10^{-10} mol of TTF per cm^2. For such systems, electrochemical measurements showed the redox signature of the bound TTF centers characterized by two reversible one-electron systems at ca. 0.40 and 0.73 V versus saturated calomel electrode (SCE). High values of electron-transfer rate constants were determined (>200 s^{-1}) and ascribed to the presence of the conjugated bridge between the attached redox-active center and the underlying silicon surface. The TTF polymer-modified surfaces prepared at 90 °C resulted from the direct grafting of polymeric structures on Si−H and/or the postattachment functionalization of the preformed TTF monolayer. Polymerization process of the TTF-terminated butadiyne derivative was also investigated in solid state by means of differential scanning calorimetry and diffuse reflectance IR spectroscopy measurements.

1. INTRODUCTION

The functionalization of oxide-free, hydrogen-terminated silicon (Si−H) surfaces using the covalent attachment of organic monolayers has received intense attention due to the large extent of potential applications with controlled and robust organic/Si interfaces.[1−6] In this context, the derivatization of Si−H surfaces with redox-active molecules (ferrocene,[7−14] metal-complexed porphyrins,[15−19] etc.) constitutes a powerful approach to the fabrication of electrically addressable devices, particularly when the goal is integrated systems devoted to information storage or transfer. For example, the integration of metal-complexed porphyrins to silicon could provide a real breakthrough in the field of molecular-based information storage.[15,16,18] Indeed, metalloporphyrins show very exciting electrochemical characteristics, such as multiple electron transfer steps at relatively low potentials, chemical stability of the different redox forms under ambient conditions, and a versatility of their redox properties depending on the nature of the complexed metal. Metalloporphyrin-modified silicon surfaces could be used as multibit information storage media with high charge density in which electrical charge is stored in multiple redox states of the bound molecules.

Another fascinating type of π-functional molecule, which has been used as a key component for various applications (sensors, receptors, switches and conductors), is tetrathiafulvalene (TTF).[20−27] From an electrochemical point of view, it shows a multiredox activity characterized by three stable redox states (namely, neutral, radical cation, and dication). Compared with metalloporphyrins, this molecule is much less sterically hindered and consequently should be immobilized on silicon with a higher surface coverage, possibly giving rise to surface-bound organic conductors or organic/inorganic hybrid materials endowed with appealing functions, such as electrocatalysis, magnetism and so on. Surprisingly, the immobilization of this electroactive molecule onto semiconducting surfaces has been scarcely developed.[28−31]

Received: March 1, 2012
Revised: May 15, 2012
Published: May 16, 2012

In a recent report, we prepared TTF monolayers covalently bound to Si−H surfaces using a TTF-terminated ethyne derivative.[29] As already demonstrated, the alkyne-derived monolayers covalently bound to silicon are usually both more densely packed and ordered than alkene-derived monolayers with a higher surface coverage.[32−35] The grafting procedure required mild conditions (90 °C) and resulted as expected in the formation of densely packed monolayers with a maximum surface coverage of ca. 5.0×10^{-10} mol of TTF per cm^2. The successful grafting of this redox-active molecule prompted us to exploit herein a new temperature-controlled functionalization route to TTF-modified Si−H surfaces. For this purpose, the synthesis of a TTF-substituted diacetylenic derivative was targeted. The presence of a second acetylenic unit offers the unique opportunity to produce both redox-active TTF monomolecular and polymer films in a reproducible and controllable manner. Indeed, TTF monolayer-modified silicon surfaces are produced when low grafting temperatures are used (typically 45 °C), whereas higher temperatures (e.g., 90 °C) lead to TTF polymer-modified surfaces. In the latter case, the generated polymer is believed to result from the polymerization of terminal diacetylenic moieties and/or silicon-bound enyne moieties, in agreement with previous studies on the polymerization of diacetylene monomers[36−43] and aromatic enynes.[44,45] It has been demonstrated that the polymer materials derived from tailor-made diacetylene derivatives showed interesting optical, spectral, and electronic properties (e.g., stress-induced colorimetric and fluorogenic transitions, sensing capabilities).[37] Moreover, a large palette of structurally organized architectures, such as supramolecular assemblies and ordered nanostructures, could be generated from these functional units. In the thematic area of the functionalization of surfaces, it has been also reported that the UV-light-induced polymerization of the grafted diacetylenic monolayer resulted in high-performance films with considerably enhanced chemical and thermal stability properties and could be used as a patterning method for producing ultrathin photoresists.[40,42]

2. EXPERIMENTAL SECTION

2.1. Reagents. Acetone (MOS electronic grade, Erbatron from Carlo Erba), anhydrous ethanol (RSE electronic grade, Erbatron from Carlo Erba), and trichloroethylene (VLSI electronic grade from Carlo-Erba) were used without further purification. The chemicals used for cleaning and etching of silicon wafer pieces (30% H_2O_2, 96−97% H_2SO_4, and 50% HF aq. solutions) were of VLSI semiconductor grade (Riedel-de-Haën). Mesitylene (>99%, Sigma-Aldrich) was passed through a neutral, activated alumina column and distilled under vacuum over sodium.

Caution: *Proper precautions must be used when handling hydrogen fluoride. Hydrogen fluoride is extremely corrosive to human tissue, contact resulting in painful, slow-healing burns. Laboratory work with HF should be conducted only in an efficient hood, with the operator wearing a full-face shield and protective clothing.*

Acetonitrile (>99.5%, puriss, over molecular sieve, Sigma-Aldrich) was used without further purification. All the syntheses were performed under an argon atmosphere using standard Schlenk techniques. The solvents were purified and dried by standard methods. The iodoMe_3TTF[46] and the 1-trimethylsilyl-buta-1,3-diyne[47] compounds were prepared according to literature procedures. NMR spectra were recorded on a Bruker AV300III spectrometer. Chemical shifts are reported in ppm referenced to TMS for ^{1}H NMR and ^{13}C NMR. Melting points were measured on a Kofler hot-stage apparatus and are uncorrected. Mass spectra were recorded with Varian MAT 311 instrument by the Centre Régional de Mesures Physiques de l'Ouest, Rennes. Elemental analysis was performed at the Centre Régional de Mesures Physiques de l'Ouest, Rennes. Column chromatography was performed using silica gel Merck 60 (70−260 mesh). Powder FT-IR spectra were recorded using a Varian-640 FT-IR spectrometer equipped with a diffuse reflectance accessory. Polarizing optical microscopy observations were performed on a Nikon Eclipse 80i polarizing microscope equipped with a Linkam LTS 420 heating stage. Differential scanning calorimetry (DSC) was carried out by using a NETZSCH DSC 200 F3 instrument equipped with an intracooler. DSC traces were measured at 10 °C/min.

*Synthesis of 1-Trimethylsilyl-buta-1,3-diyne-Substituted TTF (TTF **1**).* IodoMe_3TTF (458 mg, 1.23 mmol), $Pd(PPh_3)_2Cl_2$ (86 mg, 0.12 mmol), CuI (35 mg, 0.18 mmol), 1-trimethylsilyl-buta-1,3-diyne (300 mg, 2.46 mmol), and diisopropylamine (0.9 mL, 6.38 mmol) were added to dry and degassed tetrahydrofuran (THF) (20 mL). The reaction mixture was stirred at room temperature for 48 h. The THF was removed in vacuo, and the crude product was purified by column chromatography on a silica gel using CH_2Cl_2/petroleum ether (2/3) as eluent (R_f = 0.9). TTF **1** was isolated as orange crystals in 46% yield after slow evaporation of the solvent mixture. mp = 147 °C; ^{1}H NMR ($CDCl_3$, 300 MHz) δ 0.22 (s, 9H, $SiCH_3$), 1.94 (s, 6H, CH_3), 2.16 (s, 3H, CH_3). ^{13}C NMR ($CDCl_3$, 75 MHz) δ = 0.02, 14.1, 14.2, 16.5, 68.1, 81.1, 87.8, 94.6, 105.5, 109.6, 113.0, 123.0, 123.4, 143.9; IR $\nu_{C\equiv C}$ = 2181 (s), $\nu_{\equiv C\text{-}SiMe3}$ = 2097 cm^{-1} (s); HRMS calcd for $C_{16}H_{18}S_4Si$: 366.0061. Found: 366.0062.

*Synthesis of Buta-1,3-diyne-Substituted TTF (TTF **2**).* To a solution of TTF **1** (100 mg, 0.27 mmol) in ethanol (25 mL), a solution of KF (32 mg, 0.55 mmol) in ethanol (2 mL) was added. The reaction mixture was stirred at room temperature for 15 h under argon, and then the solvent was removed in vacuo. The residue was purified by column chromatography on a silica gel using CH_2Cl_2/petroleum ether (1/1) as eluent (R_f = 0.86). **2** was isolated as orange-brown crystals in 89% yield after slow evaporation of the solvent mixture. ^{1}H NMR δ 1.95 (s, 6H, CH_3), 2.18 (s, 3H, CH_3), 2.66 (s, 1H, C≡CH) (Figure S1, Supporting Information); ^{13}C NMR δ 13.6, 13.7, 16.0, 66.4, 67.7, 74.3, 79.9, 104.8, 108.7, 112.8, 122.5, 122.9, 144.1; IR $\nu_{C\equiv C}$ = 2201 (s), $\nu_{\equiv C-H}$ = 3280 cm^{-1} (s); HRMS calcd for $C_{13}H_{10}S_4$: 293.9665. Found 293.9664. Anal. calcd (%) for $C_{13}H_{10}S_4$ C, 53.02; H, 3.42. Found C, 52.95; H, 3.42.

Crystallography. Single-crystal X-ray diffraction data were collected on an APEX II Bruker AXS diffractometer, Mo−Kα radiation (λ = 0.71073 Å), (Centre de diffractométrie X, Université de Rennes 1, France). Structures were solved by direct methods using the SIR97 program,[48] and then refined with full-matrix least-squares methods based on F^2 (SHELX-97)[49] with the aid of the WINGX[50] program. All non-hydrogen atoms were refined with anisotropic atomic displacement parameters. H atoms were finally included in their calculated positions. Details of the final refinements are given in Table 1 for both compounds.

2.2. Preparation of TTF-Terminated *p*-type Si(100) Substrates. *TTF-Modified Flat Si(100) Surfaces.* Double-sided polished silicon Si(100) samples (*p*-type, boron-doped, 1−5 Ω cm, thickness = 250 ± 25 μm, Siltronix) were cut into 1.5 × 1.5 cm^2 pieces and sonicated for 10 min in acetone, ethanol, and

dx.doi.org/10.1021/jp302041z | J. Phys. Chem. C 2012, 116, 12093−12102

Table 1. Crystallographic Data of the Diacetylenic TTF Derivatives

compound	TTF **1**	TTF **2**
formula	$C_{16}H_{18}S_4Si$	$C_{13}H_{10}S_4$
FW ($g{\cdot}mol^{-1}$)	366.63	294.45
crystal system	monoclinic	monoclinic
space group	$C2/c$	$P2_1/n$
a (Å)	12.2489(8)	7.5140(5)
b (Å)	9.5980(8)	7.9218(8)
c (Å)	31.693(2)	22.6337(19)
α (°)	90	90
β (°)	96.914(3)	93.267(3)
γ (°)	90	90
V (Å^3)	3698.9(5)	1345.1(2)
T (K)	150(2)	150(2)
Z	8	4
D_{calc} ($g{\cdot}cm^{-3}$)	1.317	1.454
μ (mm^{-1})	0.570	0.679
total refls.	13355	8413
abs. corr .	multiscan	multiscan
uniq. refls. (R_{int})	4168(0.0671)	3025(0.0506)
unique refls.	2564 ($I > 2\sigma(I)$)	2013 ($I > 2\sigma(I)$)
R_1, wR_2	0.0594, 0.1072	0.0462, 0.0969
R_1, wR_2 (all data)	0.1101, 0.1229	0.0827, 0.1106
GoF	1.036	1.029

18.2 MΩ cm ultrapure water. They were then cleaned in 3:1 v/v concentrated H_2SO_4/30% H_2O_2 at 100 °C for 30 min, followed by copious rinsing with ultrapure water.

Caution: *The concentrated H_2SO_4:H_2O_2 (aq) piranha solution is very dangerous, particularly in contact with organic materials, and should be handled extremely carefully.*

The surface was dipped in ca. 5% HF for 2 min and dried under an argon stream without rinsing. The Si−H surface was immediately transferred into a Pyrex Schlenk tube containing TTF **2** (20 mM) in 5 mL of deoxygenated mesitylene. The solution was thoroughly purged with argon for 30 min at room temperature (rt) in the dark (aluminum foil around the glassware) and then kept at rt or heated at 45 or 90 °C under argon and ambient light for 20 h. The TTF-modified surface was rinsed with acetone and trichloroethylene, then dried under argon. The TTF-modified surfaces prepared at rt, 45, and 90 °C were denoted as Si-$\mathbf{2}_{20}$, Si-$\mathbf{2}_{45}$, and Si-$\mathbf{2}_{90}$, respectively.

TTF-Modified Porous Si(100) for Fourier Transform Infrared (FTIR) Characterization. A flat Si−H surface was prepared as described above. It was pressed against an opening in the cell bottom using a FETFE (FluoroElastomer with special TetraFluoroEthylene additives, Aldrich) O-ring seal and an ohmic contact was made on the polished rear side of the sample with the steel bottom cap (care was taken to avoid surface contamination for subsequent FTIR investigation). A platinum counter electrode was used. The hydrogen-terminated porous Si surface was produced by applying a current density of 20 mA cm^{-2} for 5 min in 50% HF/ethanol/ultrapure 18.2 MΩ cm water (2:2:1 vol.). The surface was then rinsed with ethanol and dried under an argon stream. After monitoring of the FTIR spectrum of hydrogen-terminated porous Si, the sample was again dipped in ca. 5% HF for 2 min and dried under an argon stream without rinsing. The reaction conditions of porous Si−H with TTF **2** were identical to those described for the flat Si(100) surface.

2.3. Characterization Techniques. *Electrochemical Characterizations.* Cyclic voltammetry measurements were performed with an Autolab electrochemical analyzer (PGSTAT 30 potentiostat/galvanostat from Eco Chemie B.V.) equipped with the GPES software in a homemade three-electrode Teflon cell. To avoid photoinduced electron transfer processes on silicon surfaces, all the electrochemical measurements have been performed in the dark. The working electrode, modified Si(100), was pressed against an opening in the cell bottom using a FETFE (Aldrich) O-ring seal. An ohmic contact was made on the previously polished rear side of the sample by applying a drop of an In−Ga eutectic (Alfa-Aesar, 99.99%). The electrochemically active area of the Si(100) surface was 0.3 cm^2. The counter electrode was a platinum grid, and 10^{-2} M Ag^+|Ag in acetonitrile was used as the reference electrode (+0.29 V vs aqueous saturated calomel electrode (SCE)). All reported potentials are referred to SCE (uncertainty ±0.01 V). Tetra-*n*-butylammonium perchlorate Bu_4NClO_4 was purchased from Fluka (puriss, electrochemical grade) and was used, as received, at 0.1 mol L^{-1} as the supporting electrolyte in acetonitrile. The electrolytic medium was dried over activated, neutral alumina (Merck) for 30 min, under stirring and argon atmosphere. All electrochemical measurements were carried out inside a homemade Faraday cage, at room temperature (20 ± 2 °C) and under constant argon flow. The resistance of the electrolytic cell was compensated by positive feedback.

FTIR Spectroscopy on TTF-Modified Porous Si Surfaces. FTIR spectra were acquired using a Brüker Optics Vertex 70 FT-IR spectrometer in the transmission mode (100 scans, 2 cm^{-1} resolution and automatic gain) using a DTGS detector. The porous silicon was mounted on a homemade Teflon sample holder.

Atomic Force Microscopy (AFM). AFM topography images were recorded in contact mode with a PicoSPM II microscope from Molecular Imaging using nitride silicon tips ($k \sim 0.06$ N m^{-1}) from ScienTec-Nanosensors. The thickness of the organic layers deposited on silicon surfaces was determined by the AFM "scratching" technique using n^+-type silicon tips (magnetic ac mode, NCLR Reflex, 180−193 kHz resonance frequency) from ScienTec-Nanosensors. The term "AFM scratching" is used here to describe an intentional damage to a modification layer on a relatively hard substrate. If the applied force is sufficient to disrupt the organic layer but not to damage the substrate, it is possible to "carve out" a rectangular or square trench in the deposit layer. The scratching area was achieved by moving the AFM tip in contact mode with a set-point voltage around 3 V. Then, a image at smaller magnification was recorded in intermittent contact mode, and representative line

Scheme 1. Synthesis of TTF 2

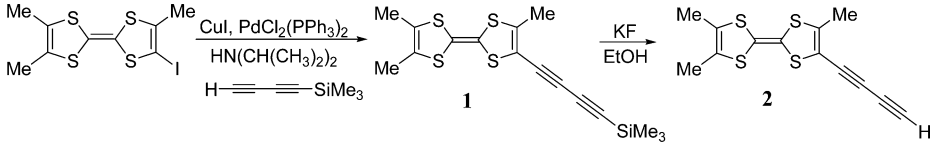

dx.doi.org/10.1021/jp302041z | J. Phys. Chem. C 2012, 116, 12093−12102

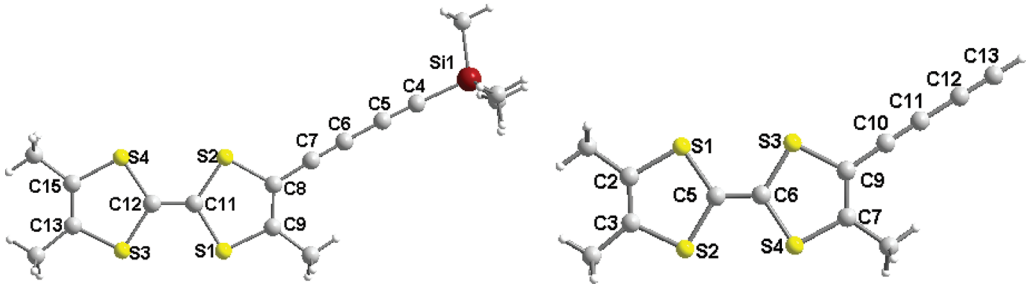

Figure 1. Molecular structure and atom numbering scheme for TTFs **1** (left) and **2** (right).

profiles through each scratch were determined (see the Supporting Information).

3. RESULTS AND DISCUSSION

3.1. Synthesis of TTF 2. The Me_3TTF-buta-1,3-diyne (TTF **2**) was prepared from iodoMe_3TTF according to the chemical pathway depicted in Scheme 1. First, TTF **1** was synthesized by a cross-coupling Sonogashira-type reaction between the iodoMe_3TTF and 1-trimethylsilylbuta-1,3-diyne catalyzed by CuI and $PdCl_2(PPh_3)_2$ in the presence of diisopropylamine. Desilylation of TTF **1** with KF in EtOH led to TTF **2** in 89% yield. Interestingly, unlike what was observed for various terminal butadiyne derivatives, TTF **2** can be purified under routine conditions and can be stored as a solid at room temperature for weeks.[51] Both TTFs **1** and **2** are electroactive molecules exhibiting two monoelectronic reversible oxidation processes which are ascribed to the formation of the TTF radical cation and dication forms. These are observed at $E^{\circ\prime}_1$ = 0.39 V vs SCE (average of anodic and cathodic peak potentials) and $E^{\circ\prime}_2$ = 0.74 V for TTF **1**, and $E^{\circ\prime}_1$ = 0.40 V and $E^{\circ\prime}_2$ = 0.75 V for TTF **2** in CH_3CN/nBu$_4$NPF$_6$ medium, while the same redox processes are observed at $E^{\circ\prime}1$ = 0.41 V and $E^{\circ\prime}2$ = 0.91 V for TTF **1**, and $E^{\circ\prime}1$ = 0.40 V and $E^{\circ\prime}2$ = 0.90 V for TTF **2** (V vs SCE) in CH_2Cl_2/nBu$_4$NPF$_6$ medium (Figure S3 in the Supporting Information). Such values are only moderately shifted toward more anodic potentials (+20 mV for TTF **2**) compared to those determined for the Me_3TTFethyne ($E^{\circ\prime}_1$ = 0.38 V and $E^{\circ\prime}_2$ = 0.88 V vs SCE, in CH_2Cl_2/nBu$_4$NPF$_6$ medium).[52] Compared with Me_3TTF-H, these two redox systems are ca. 100 mV-shifted toward more positive potentials, as a result of the weak electron-withdrawing character of the diacetylenic rod. This result is reminiscent to what was observed on disubstituted TTF-ethyne and butadiyne derivatives in which the presence of additional ethynyl spacer groups induces similar anodic shifts in the redox potentials.[53]

Single crystals of TTFs **1** and **2** suitable for an X-ray diffraction study were obtained by slow evaporation of **1** or **2** solution in dichloromethane/petroleum ether mixtures. The molecular structure of TTFs **1** and **2** are shown in Figure 1 and the X-ray packing diagrams for TTF **2** are given in Figure S2. Both TTFs, in the neutral state, exhibit a planar geometry without distortion of the dithiole rings. Investigation of the bond lengths, especially of the alkyne bonds, indicates a longer $C_{10}{\equiv}C_{11}$ bond length in TTF **2** (1.199 (4) Å) than in the related Me_3TTF-ethyne (1.152(8)Å).[54] The bond lengths of the butadiyne rod in TTF **2** $C_{10}{\equiv}C_{11}$, $C_{11}{-}C_{12}$, and $C_{12}{\equiv}C_{13}$ amount to 1.199(4), 1.376(4), and 1.177(4) Å, respectively, and are close to those observed for TTF **1**. These values are in the usual range for terminal aryl butadiynes (Table 2).[55] The butadiyne rods in both TTFs **1** and **2** are almost linear with angles at $C_9{-}C_{10}{\equiv}C_{11}$, $C_{10}{\equiv}C_{11}{-}C_{12}$, and $C_{11}{-}C_{12}{\equiv}C_{13}$ of 177.42(29)°, 178.36(29)° and 179.64(32)° for TTF **2**, respectively, and $C_8{-}C_7{\equiv}C_6$, $C_7{\equiv}C_6{-}C_5$, and $C_6{-}C_5{\equiv}C_4$ of 177.48(39)°, 178.60(41)° and 178.17(41)° for TTF **1**, respectively.

Table 2. Selected Bond Distances (Å) in TTFs 1 and 2 and Related Molecules[55]

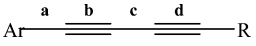

compound	*a*	*b*	*c*	*d*
TTF **1** (Ar = Me_3TTF; *R* = $SiMe_3$)	1.414(5)	1.205(5)	1.376(5)	1.208(5)
TTF **2** (Ar = Me_3TTF; *R* = H)	1.416(4)	1.199(4)	1.376(4)	1.177(4)
Ar = 4-biphenyl; *R* = H[55]	1.441(4)	1.200(4)	1.381(4)	1.180(4)
Ar = 4-pyridyl; *R* = H[55]	1.433(2)	1.202(2)	1.381(2)	1.194(2)

3.2. FTIR Spectroscopy of TTF-Modified Surfaces. Since compound **2** can efficiently be isolated, we have investigated its ability toward grafting onto oxide-free Si surfaces. First, the derivatization of oxide-free, hydrogen-terminated Si(100) surfaces by redox-active **2**-based films was investigated by FTIR spectroscopy. As already demonstrated by Zuilhof,[32,34] Gooding,[35] and co-workers, linear 1-alkynes are considerably more reactive toward either Si(100)-H or Si(111)-H than 1-alkenes, and consequently their immobilization on such surfaces requires milder conditions. Depending on the grafting temperature, we demonstrate that it is possible to produce either TTF-terminated near-monolayer or TTF polymer films through the polymerization of diacetylenic rods (*vide infra*). Transmission FTIR spectroscopy performed with modified porous Si(100) surfaces was used to probe the attachment of the TTF derivative on silicon because the chemistry of porous silicon is usually similar to that of flat silicon crystals.[56] We are conscious that the efficiency of the hydrosilylation reaction can be different with porous silicon substrates. Indeed, the reagents need to penetrate within the pores to react with the hydrogenated sites. Due to these diffusional constraints, the grafting efficiency is usually lower with porous silicon. Moreover, because of its high surface area and its complex morphology, hydrogenated porous silicon is often more sensitive to oxidation than flat silicon. In the present work, transmission FTIR spectroscopy has been used to extract qualitative information on the chemical composition of the films produced at each grafting temperature. It was not our purpose to determine quantitatively the molecular surface concentrations of different chemical bonds.

FTIR spectra of TTF-modified porous Si(100) are shown in Figure 2 as a function of the grafting temperature. For all prepared surfaces, we observe several bands in the 2500−3400 cm^{-1} region attributed to the CH_3 groups bound to the TTF

dx.doi.org/10.1021/jp302041z | J. Phys. Chem. C 2012, 116, 12093−12102

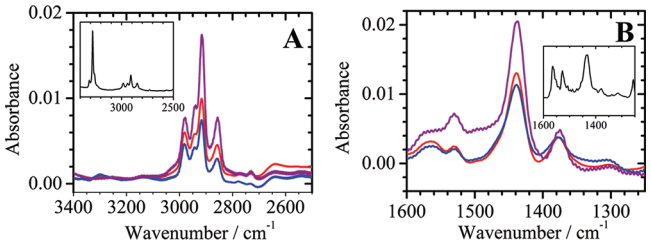

Figure 2. Transmission FTIR spectra of porous hydrogenated Si(100) after reaction with TTF **2** at rt (blue), 45 °C (red), or 90 °C (purple). The insets correspond to the FTIR spectrum of TTF **2**. The spectra were background subtracted.

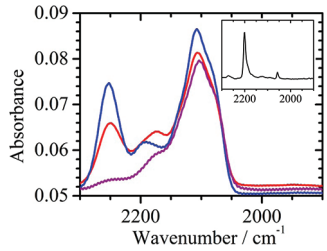

Figure 3. Transmission FTIR spectra in the 1900–2300 cm^{-1} region of porous hydrogenated Si(100) after reaction with TTF **2** at rt (blue), 45 °C (red), or 90 °C (purple). (inset: FTIR spectrum of solid TTF **2** in the same region).

moiety: the symmetric CH_3 mode at 2859 cm^{-1} and the two nondegenerate asymmetric CH_3 stretching modes at ca. 2980 and 2917 cm^{-1} (Figure 2A). Interestingly, we can notice the absence of the band corresponding to the terminal alkyne observed at 3280 cm^{-1} in the powder spectrum of TTF **2** (inset in Figure 2A and Figure S5). As shown in Scheme 2, this indicates that the binding of the TTF to the surface occurs via the hydrosilylation of the terminal alkyne leading to near-monolayer film (structure A) and not via the hydrosilylation of the disubstituted alkyne group (structure B).

Other bands are also observed in the −C═C− stretching vibration region, i.e., between 1600 and 1400 cm^{-1} (Figure 2B). The intense band at 1440 cm^{-1} can be unambiguously attributed to the C═C bonds within the TTF moieties, while the weaker band at 1565 cm^{-1} can be ascribed to the C═C units bound to the silicon surface. However, as already noticed by others[57,58] and ourselves,[59] the spectral signature for interfacial vinyl bonds is usually quite weak. Analysis of the IR spectra also revealed that the intensity of bands assigned to both the CH_3 groups and the C═C bonds of the immobilized TTF moieties increases upon increasing the grafting temperature. Such a behavior can be explained by an increase of the surface coverage of the TTF units at higher temperatures, as supported by the electrochemical data (*vide infra*).

Larger effects of the grafting temperature on the spectral response of the modified surfaces are observed in the 1900–2300 cm^{-1} region (Figure 3). Indeed, for the derivatization performed at room temperature and 45 °C, three main bands centered at ca. 2105, 2175, and 2250 cm^{-1} are clearly observed. It must be recalled that the grafting reaction with porous silicon is usually incomplete, and unreacted Si–H sites remain after the thermal reaction with TTF **2** for the three samples, as evidenced by the persistency of the broad band centered at ca. 2105 cm^{-1} corresponding to the $\nu(Si–H_x)$ stretching modes. The band observed at 2250 cm^{-1} also reveals that some Si–H sites have been oxidized into OSi–H. Comparison of the absorption intensity of this band at 2250 cm^{-1} for the monolayer obtained at room temperature with that obtained at 45 °C indicates that a larger amount of Si–H sites have been oxidized at room temperature. This trend is also in line with a smaller surface coverage of the TTF units grafted at room temperature than at 45 °C. The additional band centered at 2175 cm^{-1} is attributed to an enyne structure formed during the grafting of TTF **2** on the surface through the hydrosilylation of the terminal alkyne (Scheme 2). Such a band is observed at a slightly smaller wavenumber than that characteristic from the butadiyne structure centered at 2200 cm^{-1} (inset in Figure 3). It is interesting to note that the stretching vibration of OSi–H at 2250 cm^{-1} almost vanished from the spectrum obtained for the surface prepared at 90 °C, while the intensity of the band centered at 2175 cm^{-1} slightly decreased. Such differences can be explained by the formation of a polymeric structure onto the surface (Scheme 3). In fact, it is

Scheme 3. Polymer Formation in the Case of Si–H Reacted with TTF 2 at 90 °C

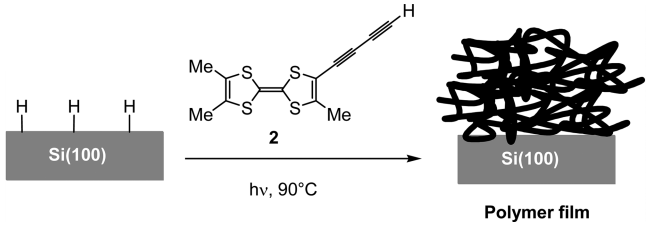

Scheme 2. Two Possible Ways for the Grafting of the Butadiyne Moiety onto Hydrogen-Terminated Si(100) Surfaces

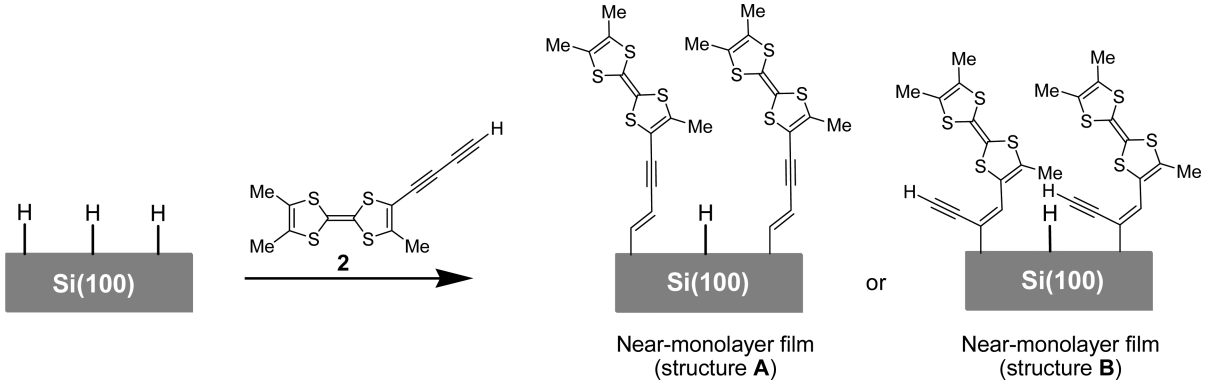

dx.doi.org/10.1021/jp302041z | J. Phys. Chem. C 2012, 116, 12093–12102

well-known that diacetylenic structures can easily undergo polymerization into enyne polymer structures upon irradiation or heat treatment.[36−43,60] The formation of polymer structures explains that the band observed at 2250 cm^{-1} is weak since the formation of a polymer network on the surface is expected to hinder the penetration of residual water and possibly O_2 into the pores of silicon and thus the oxidation of remaining Si−H sites. The weaker intensity of the vibration band at 2175 cm^{-1} can be related to the consumption of the enyne structures during the polymerization process upon light irradiation and heat treatment. Indeed, enyne derivatives such as diyne structures can undergo polymerization upon thermal treatment.[61] Therefore, the derivatization performed at 90 °C leads to the formation of a multilayered deposit on the Si surface either by the direct grafting of polymeric structures or by additional reaction of TTF **2** with the TTF fragments already grafted onto the Si surface (*vide infra*).

In order to probe whether a post-attachment functionalization of the surface is possible, a monolayer obtained at 45 °C was heated into a solution of TTF **2** in deoxygenated mesitylene, under inert atmosphere, at 90 °C for 2 days. After the usual workup, the FTIR spectrum of the modified monolayer exhibits the same characteristics as the one observed for the polymeric structure obtained at 90 °C (Figures 2 and 3, purple line). This result highlights that polymeric structures can be also produced from the thermal reaction of TTF **2** with the TTF fragments already grafted onto the Si surface. Furthermore, it is worth mentioning that no modification of the FTIR spectrum was observed when a TTF monolayer was simply heated in deoxygenated mesitylene without dissolved TTF **2** under inert atmosphere at 90 °C for 2 days. This also indicates that the monolayer is thermally stable, and that no topochemical polymerization of the enyne linkers occurs onto the surface, likely due to the lack of degree of freedom of the linker and too large intermolecular distances.

3.3. Polymerization Mechanism of the Diacetylenic TTF Derivatives Investigated by DSC. The propensity of both TTFs **1** and **2** to undergo polymerization by heat treatment in the solid state was evaluated by DSC and diffuse reflectance infrared spectroscopy. DSC experiments were carried out at a heating rate of 10 °C min^{-1} from 20 to 300 °C for TTF **1** and from 20 to 140 °C for TTF **2**. After the first heating run, the sample was cooled down to −20 °C and then a second heating run was performed (Figure 4). In the case of TTF **1**, the first heating DSC curve exhibits a strong and sharp endotherm centered at 149.9 °C, which was unambiguously attributed to the direct melting of the compound into an isotropic fluid by polarized optical microscopy. At higher temperature, a strong and broad exotherm (−58.9 kcal mol^{-1}) extending from 225.6 to 271.7 °C and centered at 255.8 °C is also observed and is attributed to an exothermic polymerization of the diacetylenic rod.[60−62] The absence of peak on the first cooling curve confirmed that the second process is irreversible. No signals are visible on the second heating process, indicating that all the starting material has been converted into the polymer during the first heating run. The first DSC heating curve measured with TTF **2** displays a single strong exotherm (−48.5 kcal mol^{-1}) extending from 108.8 to 121.9 °C and centered at 114.1 °C. In the case of TTF **2**, no melting of the compound occurs before the polymerization takes place. It appears that TTF **2** carrying a H-terminated butadiyne is much more reactive toward thermal polymerization than the silyl protected TTF derivative. The weight loss is lower than 0.1%

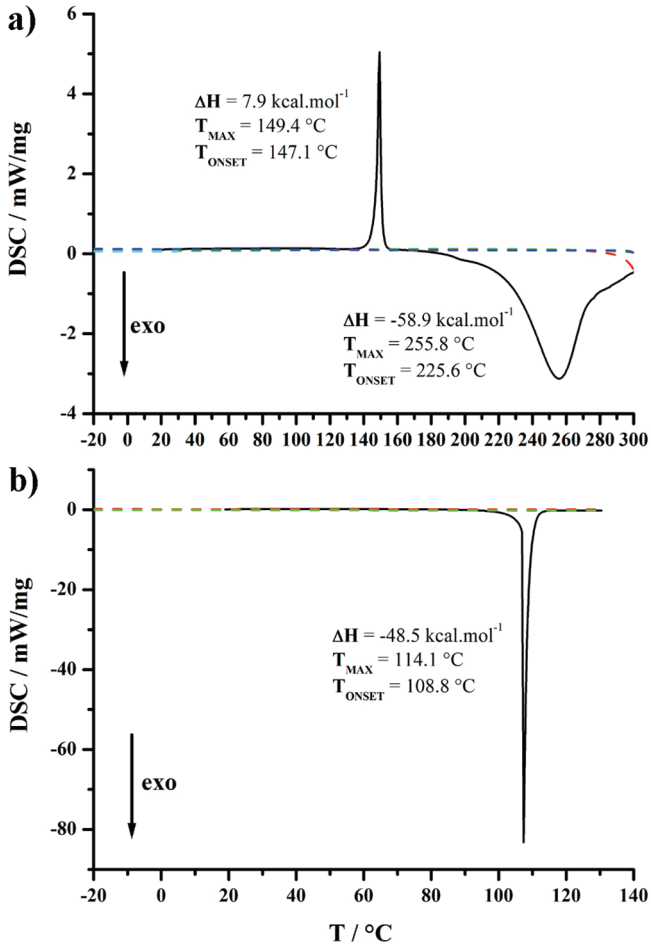

Figure 4. DSC curves for TTFs **1** (top) and **2** (bottom) at a heating rate of 10 °C min^{-1}.

after heating at 140 °C, in line with an intermolecular polymerization process involving the formation of enyne bonds. Like for TTF **1**, all the starting material is converted into the polymer and the formed polymer does not exhibit thermal reactivity in the investigated temperature range. The thermal treatment of TTFs **1** and **2** affords black powder, which was found to be completely insoluble in all the common solvents (CH_2Cl_2, toluene, DMF, DMSO), confirming the formation of a polymeric material after thermal treatment.

The heat-treated samples were analyzed by FTIR spectroscopy. In the IR spectrum of TTF **2** heated at 140 °C, the stretching vibration bands of the C−H ($\nu_{\equiv C-H}$ at 3278 cm^{-1}) and the terminal C≡C bonds ($\nu_{C\equiv C}$ at 2200 cm^{-1}) are no longer visible. Instead, a new vibration band is observed at 2175 cm^{-1}, which is attributed to the vibration band of the C≡C bonds of the enyne units formed during the polymerization (Figure S6). As shown in Scheme 4, two plausible structures for an enyne polymer can be envisaged. Since no stretching vibration bands of a terminal alkyne ($\nu_{\equiv C-H}$) are visible on the IR spectrum, we assume that mainly the polymer P_A is formed during the thermally activated polymerization process. In light of these investigations, a P_A-type polymer is most likely formed on the Si surface during the derivatization of Si−H by TTF **2** at 90 °C.

3.4. AFM Characterization of the TTF-Modified Si(100) Surfaces. Figure 5 shows the AFM images of the TTF-modified flat Si(100) surfaces prepared at different temper-

dx.doi.org/10.1021/jp302041z | J. Phys. Chem. C 2012, 116, 12093−12102

Scheme 4. Thermal Polymerization of TTF 2

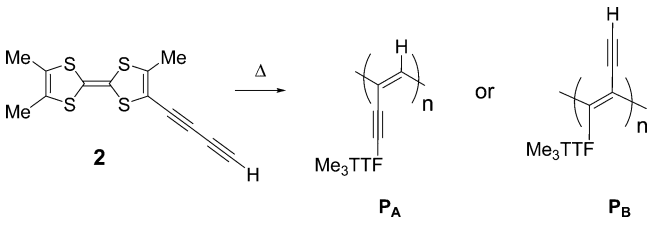

atures. These are characterized by homogeneously distributed and densely packed globular features with root-mean-square (rms) roughness values of 4.4, 8.0, and 50 Å (averaged on several images) measured for Si-$\mathbf{2}_{20}$, Si-$\mathbf{2}_{45}$ and Si-$\mathbf{2}_{90}$, respectively. Such values are much higher than the roughness determined for Si−H, namely, 0.5 Å, and are therefore indicative of the surface modification. Approximative film thicknesses were obtained by the commonly used AFM "scratching" technique.[63] Values of 1.3 ± 0.8 nm, 2.7 ± 0.1 nm, and higher than 140 nm were determined for Si-$\mathbf{2}_{20}$, Si-$\mathbf{2}_{45}$ and Si-$\mathbf{2}_{90}$, respectively (Figure S7). Taking into account some drawbacks of the AFM "scratching" method (e.g., edge irregularities due to the torsion of the cantilever, or postscratching modification due to the dragging of the surface), the two first values that are in the range of the length of the molecule are consistent with the formation of monolayers, whereas the thickness obtained at 90 °C can be unambiguously attributed to the formation of a multilayered system. This observation is also confirmed by the electrochemical data (see the next section).

3.5. Electrochemical Characterization of the TTF-Modified Si(100) Surfaces. The cyclic voltammetry characterization of the TTF-modified flat Si(100) surfaces in thoroughly dried acetonitrile medium reveals the presence of two perfectly reversible one-electron systems attributed to the formation of the TTF radical cation and dication, respectively (Figure 6). The oxidation potentials are observed at $E^{\circ\prime}_1$ = 0.40 V and $E^{\circ\prime}_2$ = 0.73 V vs SCE in the case of Si-$\mathbf{2}_{20}$ and Si-$\mathbf{2}_{45}$, which is consistent with the values determined for TTF **2** in solution, namely, 0.40 and 0.75 V. By contrast, the oxidation of the TTF units in Si-$\mathbf{2}_{90}$ is shifted to more positive potentials, $E^{\circ\prime}_1$ = 0.47 V and $E^{\circ\prime}_2$ = 0.78 V. From the area under either the anodic or cathodic scan (involving two electrons), the surface coverage of attached TTF units can be estimated at (2.0 ± 0.2) × 10^{-10}, (5.4 ± 0.4) × 10^{-10} and (2.5 ± 0.2) × 10^{-8} mol cm^{-2} for Si-$\mathbf{2}_{20}$, Si-$\mathbf{2}_{45}$ and Si-$\mathbf{2}_{90}$, respectively. Considering the TTF molecules as rectangular blocks,[64−66] the theoretical maximum coverage expected for TTF monomolecular films is 4.0−5.0 × 10^{-10} mol cm^{-2}. This indicates the formation of a densely packed TTF monolayer in the case of Si-$\mathbf{2}_{45}$, whereas the grafting at 20 and 90 °C yields submonolayer and multilayer films, respectively. Consistent with that, both anodic and cathodic peak current intensities corresponding to the two systems of Si-$\mathbf{2}_{20}$ and Si-$\mathbf{2}_{45}$ are found to be directly proportional to the potential scan rate v within the 0.0 to ca. 1.0 V s^{-1} range, as expected for surface-confined redox species.[67] By contrast, the linearity range for Si-$\mathbf{2}_{90}$ is much narrower, with a deviation from linearity observed for scan rates higher than 0.05 V s^{-1}. Such a deviation from linearity is expected when the overall electrochemical process is limited by the rate of mass transport on the time scale of the cyclic voltammetry experiment. In the case of Si-$\mathbf{2}_{90}$, this situation can be caused by the restricted mobility of the electrolyte counteranions through the thick film to ensure the electroneutrality of the oxidized material.

Apparent rate constants for electron transfer of bound TTF units, k_{app}, was calculated for the thin layers (i.e., Si-$\mathbf{2}_{20}$ and Si-$\mathbf{2}_{45}$) using Laviron's formalism (eq 1)[68] based on the classical Butler−Volmer theory. Upon increasing v, the anodic peak potentials corresponding to the two redox processes of bound TTF, E_{pa_1} and E_{pa_2}, shift in the positive direction relative to $E^{\circ\prime}$, which reflects control of the voltammetry by the rate of electron transfer of the TTF units (Figure 7).

$$k_{app} = (1 - \alpha)nFv_a/RT \quad (1)$$

where α is the charge transfer coefficient and v_a is the intersection of the two linear regions in the graph E_{pa} vs log v obtained at low and high scan rates. Assuming α = 0.5 for both processes, the slope of the linear E_{pa}−log v part at high v is therefore equal to 2.3 $RT/(1 - \alpha)nF$, i.e., 116 mV per decade of v at 293 K.[68] From the variation of E_{pa_1} and E_{pa_2} with log v, the k_{app} values for the TTF/$TTF^{\bullet+}$ and $TTF^{\bullet+}$/TTF^{2+} redox couples are estimated to be 240 and 475 s^{-1} for Si-$\mathbf{2}_{20}$, while

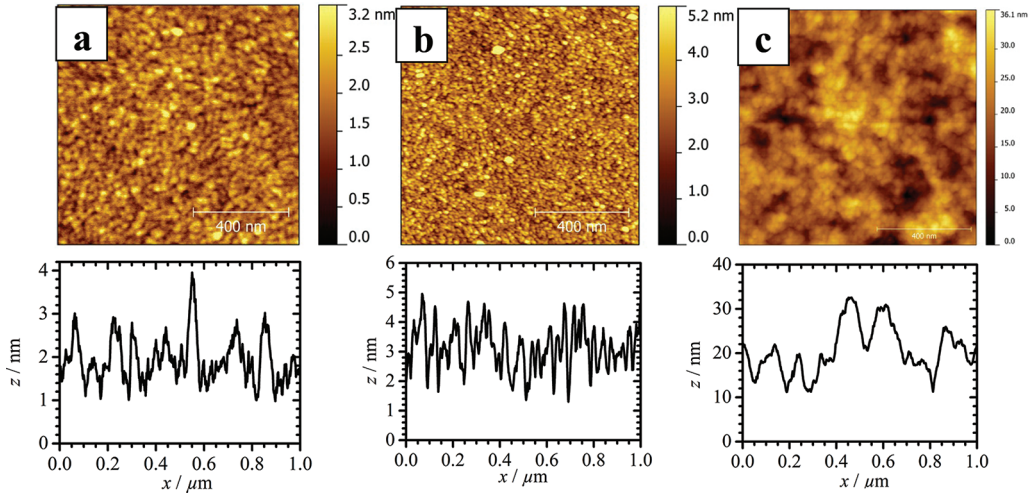

Figure 5. Contact-mode AFM images and corresponding cross-section profiles (taken in the middle of the images) of TTF-modified surfaces prepared at 20 °C (a), 45 °C (b), and 90 °C (c). Size: 1 × 1 μm^2.

dx.doi.org/10.1021/jp302041z | J. Phys. Chem. C 2012, 116, 12093−12102

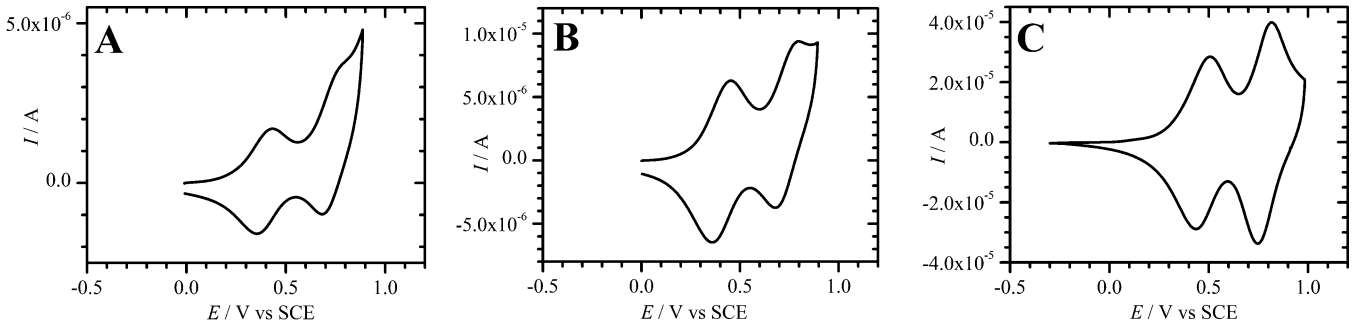

Figure 6. Cyclic voltammograms in CH_3CN + 0.1 M Bu_4NClO_4 of Si-$\mathbf{2}_{20}$ (A, 0.1 V s^{-1}), Si-$\mathbf{2}_{45}$ (B, 0.1 V s^{-1}), and Si-$\mathbf{2}_{90}$ (C, 0.01 V s^{-1}).

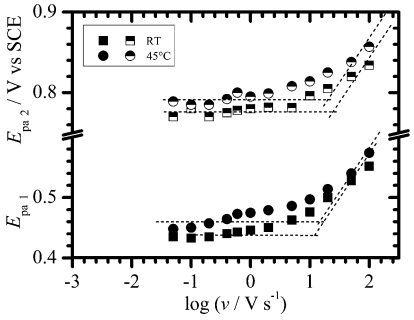

Figure 7. E_{pa}–log v plots for both redox processes of the attached TTF determined from cyclic voltammograms in CH_3CN + 0.1 M Bu_4NClO_4 of Si-$\mathbf{2}_{20}$ and Si-$\mathbf{2}_{45}$. The values have been corrected from the resistance of the electrolytic cell.

values of 270 and 400 s^{-1} are calculated for Si-$\mathbf{2}_{45}$. These high values can be ascribed to the presence of the conjugated bridge between the attached redox-active center and the underlying silicon surface and are considerably higher than those previously reported for TTF monolayers bound to semiconducting surfaces through a saturated spacer.[28] Also interestingly, the so-called acceleration phenomenon observed for the second electron transfer process of TTF is thought to be caused by environmental effects such as the formation of ion pairs between the oxidized TTF moieties and the electrolyte anions, as already reported for similar redox-active monolayers.[28,65]

The electrochemical stability of these redox-active surfaces has been also examined and was found to be sensitive to the used potential window, as exemplified for the surface Si-$\mathbf{2}_{45}$. Si-$\mathbf{2}_{45}$ shows an electroactivity loss of ca. 25% after 200 cycles at 0.2 V s^{-1} when the potential is scanned up to the second redox process, i.e., 0.9 V vs SCE (Figure 8). A repetitive scanning

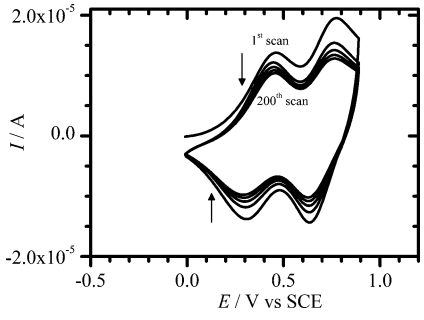

Figure 8. Electrochemical stability over 200 cycles of Si-$\mathbf{2}_{45}$ at 0.2 V s^{-1} in CH_3CN + 0.1 M Bu_4NClO_4 with one trace every 50 scans.

limited to the first redox system results in an electroactivity loss of only 15%. The lowest stability of the second redox process can be explained by the highest reactivity of the electrogenerated TTF dication toward some nucleophilic species present in the electrolytic medium.

4. CONCLUSIONS

In summary, we have synthesized and demonstrated the versatility of the TTF-terminated butadiyne as a key precursor for the preparation of either TTF monolayer- or TTF polymer-modified silicon surfaces depending on the temperature used for the grafting onto hydrogen-terminated Si(100) surfaces. Densely packed monolayers were obtained at 45 °C with a maximum coverage of ca. 5.4 × 10^{-10} mol cm^{-2}, which is a value close to that found for the grafting of the TTF-terminated ethyne derivative (5.0 × 10^{-10} mol cm^{-2}) at 90 °C.[29] This similar surface coverage obtained in milder conditions herein indicates the highest reactivity of the butadiyne derivative toward hydrogen terminated Si(100) surfaces. Characterization of the near-monolayer-modified silicon surfaces by IR spectroscopy provides evidence that TTF is bound to the surface through the formation of enyne linkers via hydrosilylation of the terminal alkyne bond. Interestingly, the rate constants for electron transfer of bound TTF units (>200 s^{-1}) were considerably higher than those previously reported for TTF monolayers bound to semiconducting surfaces through a saturated spacer.[28] Such high values were ascribed to the presence of the conjugated bridge between the attached redox-active center and the underlying silicon surface. Thanks to the thermal topochemical polymerization of the butadiyne rod, we also prepared TTF polymer-modified surfaces at 90 °C by direct grafting of polymeric structures on Si–H sites and/or the postattachment functionalization of the preformed TTF monolayer. This polymerization reaction resulted in electroactive films with surface coverages of attached TTF units higher than 2.0 × 10^{-8} mol cm^{-2}. This postattachment functionalization strategy involving redox-active monolayers bound to the surface through enyne linkers could be exploited to attach different functional groups other than TTF (e.g., electron acceptors) onto the silicon surface. Work directed toward this stimulating prospect is currently underway.

■ ASSOCIATED CONTENT

Supporting Information

^{1}H NMR spectrum and X-ray packing diagram of TTF **2**, cyclic voltammetry characterizations of TTFs **1** and **2**, FTIR spectra of solid TTFs **1**, **2**, and **2** after DSC measurements, AFM images of the **2**-modified surfaces, and X-ray crystallographic

dx.doi.org/10.1021/jp302041z | J. Phys. Chem. C 2012, 116, 12093–12102

files in CIF format for TTFs **1** and **2**. This material is available free of charge via the Internet at http://pubs.acs.org.

AUTHOR INFORMATION

Corresponding Author

*E-mail: fabre@univ-rennes1.fr; tel +33 (0) 2 2323 6550; fax +33 (0) 2 2323 6732 (B.F.). E-mail: dominique.lorcy@univ-rennes1.fr; tel +33 (0) 2 2323 6273; fax +33 (0) 2 2323 6738 (D.L.).

Notes

The authors declare no competing financial interest.

ACKNOWLEDGMENTS

Financial support from the CNRS is gratefully acknowledged. G.Y. thanks Ministère de la Recherche for his Ph.D. grant.

REFERENCES

(1) Buriak, J. M. *Chem. Rev.* **2002**, *102*, 1271−1308.
(2) Wayner, D. D. M.; Wolkow, R. A. *J. Chem. Soc., Perkin Trans. 2* **2002**, 23−34.
(3) Ciampi, S.; Harper, J. B.; Gooding, J. J. *Chem. Soc. Rev.* **2010**, *39*, 2158−2183.
(4) Linford, M. R.; Fenter, P.; Eisenberger, P. M.; Chidsey, C. E. D. *J. Am. Chem. Soc.* **1995**, *117*, 3145−3155.
(5) Boukherroub, R. *Curr. Opin. Solid State Mater. Sci.* **2005**, *9*, 66−72.
(6) Ashwell, G. J.; Phillips, L. J.; Robinson, B. J.; Urasinska-Wojcik, B.; Lambert, C. J.; Grace, I. M.; Bryce, M. R.; Jitchati, R.; Tavasli, M.; Cox, T. I.; et al. *ACS Nano* **2010**, *4*, 7401−7406.
(7) Fabre, B. *Acc. Chem. Res.* **2010**, *43*, 1509−1518.
(8) Cummings, S. P.; Savchenko, J.; Ren, T. *Coord. Chem. Rev.* **2011**, *255*, 1587−1602.
(9) Zigah, D.; Herrier, C.; Scheres, L.; Giesbers, M.; Fabre, B.; Hapiot, P.; Zuilhof, H. *Angew. Chem., Int. Ed.* **2010**, *49*, 3157−3160.
(10) Hauquier, F.; Ghilane, J.; Fabre, B.; Hapiot, P. *J. Am. Chem. Soc.* **2008**, *130*, 2748−2749.
(11) Fabre, B.; Hauquier, F. *J. Phys. Chem. B* **2006**, *110*, 6848−6855.
(12) Decker, F.; Cattaruzza, F.; Coluzza, C.; Flamini, A.; Marrani, A. G.; Zanoni, R.; Dalchiele, E. A. *J. Phys. Chem. B* **2006**, *110*, 7374−7379.
(13) Dalchiele, E. A.; Aurora, A.; Bernardini, G.; Cattaruzza, F.; Flamini, A.; Pallavicini, P.; Zanoni, R.; Decker, F. *J. Electroanal. Chem.* **2005**, *579*, 133−142.
(14) Tajimi, N.; Sano, H.; Murase, K.; Lee, K.-H.; Sugimura, H. *Langmuir* **2007**, *23*, 3193−3198.
(15) Lindsey, J. S.; Bocian, D. F. *Acc. Chem. Res.* **2011**, *44*, 638−650.
(16) Roth, K. M.; Yasseri, A. A.; Liu, Z.; Dabke, R. B.; Malinovskii, V.; Schweikart, K.-H.; Yu, L.; Tiznado, H.; Zaera, F.; Lindsey, J. S.; et al. *J. Am. Chem. Soc.* **2003**, *125*, 505−517.
(17) Yasseri, A. A.; Syomin, D.; Loewe, R. S.; Lindsey, J. S.; Zaera, F.; Bocian, D. F. *J. Am. Chem. Soc.* **2004**, *126*, 15603−15612.
(18) Liu, Z.; Yasseri, A. A.; Lindsey, J. S.; Bocian, D. F. *Science* **2003**, *302*, 1543−1545.
(19) Huang, K.; Duclairoir, F.; Pro, T.; Buckley, J.; Marchand, G.; Martinez, E.; Marchon, J.-C.; De Salvo, B.; Delapierre, G.; Vinet, F. *ChemPhysChem* **2009**, *10*, 963−971.
(20) Canevet, D.; Sallé, M.; Zhang, G.; Zhang, D.; Zhu, D. *Chem. Commun.* **2009**, 2245−2269.
(21) Batail, P. *Chem. Rev.* **2004**, *104*, 4887−5781 Special issue on Molecular Conductors.
(22) Coskun, A.; Spruell, J. M.; Barin, G.; Fahrenbach, A. C.; Forgan, R. S.; Colvin, M. T.; Carmieli, R.; Benítez, D.; Tkatchouk, E.; Friedman, D. C.; et al. *J. Am. Chem. Soc.* **2011**, *133*, 4538−4547.
(23) Klajn, R.; Stoddart, J. F.; Grzybowski, B. A. *Chem. Soc. Rev.* **2010**, *39*, 2203−2237.
(24) Bryce, M. R. *J. Mater. Chem.* **2000**, *10*, 589−598.
(25) Nielsen, M. B.; Lomholt, C.; Becher, J. *Chem. Soc. Rev.* **2000**, *29*, 153−164.
(26) Segura, J. L.; Martín, N. *Angew. Chem., Int. Ed.* **2001**, *40*, 1372−1409.
(27) Martín, N.; Sanchez, L.; Herranz, M. A.; Illescas, B.; Guldi, D. M. *Acc. Chem. Res.* **2007**, *40*, 1015−1024.
(28) Bellec, N.; Faucheux, A.; Hauquier, F.; Lorcy, D.; Fabre, B. *Int. J. Nanotechnol.* **2008**, *5*, 741−756.
(29) Yzambart, G.; Fabre, B.; Lorcy, D. *Langmuir* **2012**, *28*, 3453−3459.
(30) Ohnuki, H.; Izumi, M.; Lenfant, S.; Guerin, D.; Imakubo, T.; Vuillaume, D. *Appl. Surf. Sci.* **2005**, *246*, 392−396.
(31) Simão, C.; Mas-Torrent, M.; Casado-Montenegro, J.; Oton, F.; Veciana, J.; Rovira, C. *J. Am. Chem. Soc.* **2011**, *133*, 13256−13259.
(32) Scheres, L.; Giesbers, M.; Zuilhof, H. *Langmuir* **2010**, *26*, 4790−4795.
(33) Scheres, L.; Rijksen, B.; Giesbers, M.; Zuilhof, H. *Langmuir* **2011**, *27*, 972−980.
(34) Scheres, L.; Giesbers, M.; Zuilhof, H. *Langmuir* **2010**, *26*, 10924−10929.
(35) Ng, A.; Ciampi, S.; James, M.; Harper, J. B.; Gooding, J. J. *Langmuir* **2009**, *25*, 13934−13941.
(36) Cantow, H. J. *Polydiacetylenes*; Springer-Verlag: New York, 1984.
(37) Yarimaga, O.; Jaworski, J.; Yoon, B.; Kim, J.-M. *Chem. Commun.* **2012**, *48*, 2469−2485 and references therein..
(38) Lee, J.; Yarimaga, O.; Lee, C. H.; Choi, Y.-K.; Kim, J.-M. *Adv. Funct. Mater.* **2011**, *21*, 1032−1039.
(39) Cho, S.; Han, G.; Kim, K.; Sung, M. M. *Angew. Chem., Int. Ed.* **2011**, *50*, 2742−2746.
(40) Kim, T.; Chan, K. C.; Crooks, R. M. *J. Am. Chem. Soc.* **1997**, *119*, 189−193.
(41) Xu, Z.; Byun, H.-S.; Bittman, R. *J. Org. Chem.* **1991**, *56*, 7183−7186.
(42) Batchelder, D. N.; Evans, S. D.; Freeman, T. L.; Häussling, L.; Ringsdorf, H.; Wolf, H. *J. Am. Chem. Soc.* **1994**, *116*, 1050−1053.
(43) Tieke, B.; Wegner, G.; Naegele, D.; Ringsdorf, H. *Angew. Chem., Int. Ed. Engl.* **1976**, *15*, 764−765.
(44) Ochiai, B.; Tomita, I.; Endo, T. *Macromolecules* **2002**, *35*, 597−601.
(45) Ochiai, B.; Tomita, I.; Endo, T. *Macromolecules* **2001**, *34*, 1634−1639.
(46) John, D. E.; Moore, A. J; Bryce, M. R.; Batsanov, A. S.; Howard, J. A. K. *Synthesis* **1998**, 826−828.
(47) (a) Holmes, A. B.; Jennings-White, C. L. D.; Schulthess, A. H.; Akinde, B.; Walton, D. R. M. *J. Chem. Soc., Chem. Commun.* **1979**, 840−842. (b) Holmes, A. B.; Jones, G. E. *Tetrahedron Lett.* **1980**, *21*, 3111−3112.
(48) Altomare, A.; Burla, M. C.; Camalli, M.; Cascarano, G.; Giacovazzo, C.; Guagliardi, A.; Moliterni, A. G. G.; Polidori, G.; Spagna, R. *J. Appl. Crystallogr.* **1999**, *32*, 115−119.
(49) Sheldrick, G. M. *Acta Crystallogr.* **2008**, *A64*, 112−122.
(50) Farrugia, L. J. *J. Appl. Crystallogr.* **1999**, *32*, 837−838.
(51) Morisaki, Y.; Luu, T.; Tywinski, R. R. *Org. Lett.* **2006**, *8*, 689−692.
(52) Vacher, A.; Barrière, F.; Roisnel, T.; Lorcy, D. *Chem. Commun.* **2009**, 7200−7202.
(53) Wang, C.; Pålsson, L.-O.; Batsanov, A. S.; Bryce, M. R. *J. Am. Chem. Soc.* **2006**, *128*, 3789−3799.
(54) Vacher, A.; Barrière, F.; Piekara-Sady.; Roisnel, T.; Lorcy, D. *Organometallics* **2011**, *30*, 3570−3578.
(55) West, K.; Wang, C.; Batsanov, A. S.; Bryce, M. R. *J. Org. Chem.* **2006**, *71*, 8541−8544.
(56) (a) Lee, E. J.; Ha, J. S.; Sailor, M. J. *J. Am. Chem. Soc.* **1995**, *117*, 8295−8296. (b) Kim, N. Y.; Laibinis, P. E. *J. Am. Chem. Soc.* **1997**, *119*, 2297−2298. (c) Bateman, J. E.; Eagling, R. D.; Worrall, D. R.; Horrocks, B. R.; Houlton, A. *Angew. Chem., Int. Ed.* **1998**, *37*, 2683−2685.
(57) Cicero, R. L.; Linford, M. R.; Chidsey, C. E. D. *Langmuir* **2000**, *16*, 5688−5695.

(58) Stewart, M. P.; Buriak, J. M. *Angew. Chem., Int. Ed.* **1998**, *37*, 3257−3260.
(59) Gauthier, N.; Argouarch, G.; Paul, F.; Humphrey, M. G.; Toupet, L.; Ababou-Girard, S.; Sabbah, H.; Hapiot, P.; Fabre, B. *Adv. Mater.* **2008**, *20*, 1952−1956.
(60) Carré, F.; Devylder, N.; Dutremez, S. G.; Guérin, C.; Henner, B. J. L.; Jolivet, A.; Tomberli, V. *Organometallics* **2003**, *22*, 2014−2033.
(61) Gandon, S.; Mison, P.; Sillion, B. *Polymer* **1997**, *38*, 1449−1459.
(62) Corriu, R. J. P.; Gerbier, P.; Guérin, C.; Henner, B. J. L.; Jean, A.; Mutin, P. H. *Organometallics* **1992**, *11*, 2507−2513.
(63) (a) Anariba, F.; DuVall, S. H.; McCreery, R. L. *Anal. Chem.* **2003**, *75*, 3837−3844. (b) Nishikawa, T.; Nishida, J.; Ookura, R.; Nishimura, S.-I.; Scheumann, V.; Zizlsperger, M.; Lawall, R.; Knoll, W.; Shimomura, M. *Langmuir* **2000**, *16*, 1337−1342. (c) Wang, D.; Buriak, J. M. *Surf. Sci.* **2005**, *590*, 154−161. (d) Li, Y.-H.; Buriak, J. M. *Inorg. Chem.* **2006**, *45*, 1096−1102.
(64) Ditzler, L. R.; Karunatilaka, C.; Donuru, V. R.; Liu, H. Y.; Tivanski, A. V. *J. Phys. Chem. C* **2010**, *114*, 4429−4435.
(65) Yokota, Y.; Miyazaki, A.; Fukui, K.-i.; Enoki, T.; Tamada, K.; Hara, M. *J. Phys. Chem. B* **2006**, *110*, 20401−20408.
(66) Yip, C. M.; Ward, M. D. *Langmuir* **1994**, *10*, 549−556.
(67) Bard, A. J.; Faulkner, L. R. *Electrochemical Methods. Fundamentals and Applications*; Wiley: New York, 1980; p 522.
(68) Laviron, E. *J. Electroanal. Chem.* **1979**, *101*, 19−28.